Cellular and Molecular Life Sciences (2024) 81:21
https://doi.org/10.1007/s00018-023-05042-w

ORIGINAL ARTICLE

Delineating the mechanism of fragility at *BCL6* breakpoint region associated with translocations in diffuse large B cell lymphoma

Vidya Gopalakrishnan[1,2,3] · Urbi Roy[1] · Shikha Srivastava[1,4] · Khyati M. Kariya[1] · Shivangi Sharma[1] · Saniya M. Javedakar[1] · Bibha Choudhary[2] · Sathees C. Raghavan[1]

Received: 7 June 2023 / Revised: 5 November 2023 / Accepted: 7 November 2023

Abstract

BCL6 translocation is one of the most common chromosomal translocations in cancer and results in its enhanced expression in germinal center B cells. It involves the fusion of *BCL6* with any of its twenty-six Ig and non-Ig translocation partners associated with diffuse large B cell lymphoma (DLBCL). Despite being discovered long back, the mechanism of *BCL6* fragility is largely unknown. Analysis of the translocation breakpoints in 5′ UTR of *BCL6* reveals the clustering of most of the breakpoints around a region termed Cluster II. In silico analysis of the breakpoint cluster sequence identified sequence motifs that could potentially fold into non-B DNA. Results revealed that the Cluster II sequence folded into overlapping hairpin structures and identified sequences that undergo base pairing at the stem region. Further, the formation of cruciform DNA blocked DNA replication. The sodium bisulfite modification assay revealed the single-strandedness of the region corresponding to hairpin DNA in both strands of the genome. Further, we report the formation of intramolecular parallel G4 and triplex DNA, at Cluster II. Taken together, our studies reveal that multiple non-canonical DNA structures exist at the *BCL6* cluster II breakpoint region and contribute to the fragility leading to BCL6 translocation in DLBCL patients.

Keywords Chromosomal translocations · Translocation breakpoint · Double-strand break · Lymphoid cancer · Genomic fragility · Non-B DNA · G4 DNA · Cruciform DNA · Triplex DNA

Introduction

Diffuse large B cell lymphoma (DLBCL) is the most frequent and aggressive form of non-Hodgkin lymphomas, that accounts for approximately 40% of cases globally [50]. Among several chromosomal translocations reported in DLBCL, the most common are those involving *BCL6,* which occurs in ~ 50% of DLBCL cases [54].

✉ Bibha Choudhary
vibha@ibab.ac.in

✉ Sathees C. Raghavan
sathees@iisc.ac.in

1 Department of Biochemistry, Indian Institute of Science, Bangalore 560 012, India

2 Institute of Bioinformatics and Applied Biotechnology, Electronics City, Bangalore 560 100, India

3 Department of Zoology, St. Joseph's College (Autonomous), Irinjalakuda, Kerala 680121, India

4 Department of Bioscience and Biotechnology, Banasthali Vidyapith, Tonk, Rajasthan 304022, India

The BCL6 gene located in chromosome 3q27, spans 26 kb and contains 10 exons, with the protein synthesis initiation signal localized in exon 3, while zinc finger motifs are located in exons 6–9 [17, 58]. It encodes a sequence-specific transcription repressor, BCL6 that aids germinal center formation in B cells [58]. BCL6 is tightly regulated during B-cell differentiation, wherein it aids somatic hypermutation of immunoglobulin genes and prevents the exit of B cells from GC reaction and plasma-cell differentiation [41]. BCL6 overexpression makes these cells resistant to massive proliferation and to the mutagenic effect of the DNA-editing enzymes that facilitate immunoglobulin affinity maturation [20]. It is downregulated in cells that exit the germinal centers, necessary for B cell differentiation and apoptosis. BCL6 has been shown to play a critical role in B–T-cell interaction [39]. TP53 (Tumor Protein P53), the gene that codes for p53 tumor suppressor protein, is a direct target of BCL6, which provided the first evidence that BCL6 protects cells against DNA damage induced apoptosis [43].

Rearrangement of the *BCL6* gene on chromosome 3 is observed in 40% of DLBCL and around 5–10% of Follicular

Published online: 10 January 2024

lymphoma (FL) patients [59]. *BCL6* undergoes translocation with different partner chromosomes, including *Ig* loci (Chromosome 14), leading to its constitutive expression in germinal center B cells [13] (Fig. S1A). The breakpoint cluster lies within a 4 kb region that spans the promoter, the first non-coding exon, and the first intron of the gene resulting in the fusion of exons 2–10 with the partner genes which brings it under the control of heterologous promoters leading to BCL6 overexpression, thus playing a critical role in lymphomagenesis. Analysis of *BCL6* translocation breakpoints clustered in a 2156-bp segment of intron 1 revealed the prevalence of Ig-BCL6 translocations at Activation-Induced cytosine Deaminase (AID) hotspots (WGCW and WRC) (W = A/T, R = A/G), while the *BCL6* juxtaposition with non-Ig genes were favored at CpG/CGC sites [28]. It was speculated that both WGCW/WRC and CpG/CGC breaks at *BCL6* could be initiated by AID expressed in germinal center B cells, leading to gene rearrangements and pathogenesis of *BCL6* in DLBCL [28].

Studies have shown that somatic hypermutation (SHM) leads to deleterious mutations in the 5′ regulatory region of *BCL6*, which in turn leads to the development of DLBCL by blocking post germinal-centre differentiation [51]. These point mutations are observed independent of translocations in about 60% of DLBCL cases [42]. Subsequent studies have shown that a subset of DLBCL carrying specific activating mutations in 5′ regulatory region of *BCL6* can disrupt its autoregulatory circuit [55] and impair IR4 mediated repression [47]. One of the major causes of chromosomal fragility is the prevalence of non-B DNA structures in the human genome [46]. Alternative DNA structures exist in all forms of life [44]. Non-B DNA structures are more prone to DNA breaks than standard B DNA owing to its single-strandedness and subsequent action of structure-specific nucleases. The structural transitions that facilitate the non-canonical structures occur during DNA replication or transcription that involves local unwinding of DNA strands.

Cruciform or hairpin DNA, consisting of a branch point, a stem and a loop requires inverted repeats of six or more nucleotides in the DNA sequence for its formation [27]. Presence of palindromic AT-rich repeats (PATRRs) induces cruciform formation [27]. Whereas stretches of guanines separated by other bases has an inherent propensity to self-associate and form four stranded helical structures called G-quadruplexes or G-tetrads [14]. The formation of triplex DNA occurs when pyrimidine or purine bases occupying the major groove of the DNA double helix forms Hoogsteen base pairs with purines of Watson–crick base pairs [11]. The presence of these non-B DNA structures in the genome have been mapped to breakpoint regions leading to chromosomal translocations in several leukemia and lymphomas [35]. Previous studies have suggested that the formation of a non-B DNA structure at *BCL2* MBR (Major Breakpoint Region), makes the region prone to RAG mediated cleavage at single-double-stranded transitions of the structure [18, 34]. The BCL2 MBR was shown to fold into a G-quadruplex structure, thereby contributing to t(14,18) [34, 35]. Similarly, DNA sequence capable of forming non-B DNA structures (H-DNA, G4 DNA) in the human *c-MYC* loci colocalizes with the translocation breakpoints and undergo frequent DSBs in mammalian cells [9]. Presence of G4 DNA structures are also shown at *HOX11* breakpoint region, resulting in t(10;14) translocation [38]. Further, it was also found that > 50% of the translocation breakpoint region indeed possess G4 motifs, and there is a close association between CpGs, nonamers and translocation break point regions [19].

In the current study, we have investigated the mechanism that contributes towards the fragility of *BCL6* gene during translocation leading to DLBCL. In DLBCL, the majority of the *BCL6* translocations occur in the 3.3-kb region termed the major translocation cluster (MTC) that covers the first noncoding exon 1 and the 5′ region of intron 1 of *BCL6* locus. The adjoining major mutation cluster (MMC), located at the exon–intron boundary, is the physiological target for somatic hypermutation (SHM). The first intron of *BCL6* is a highly conserved region and together with the first non-coding exon, contains the proposed regulatory elements at its 5′ extremity. The intron region also displays frequent genetic aberrations in lymphomas [17]. Interestingly, most of the breakpoints in *BCL6* gene observed during DLBCL are part of the MTC and was thus analyzed further in our study. Based on the distribution of breakpoints at this 4 Kb region spanning the 5′UTR of the *BCL6* gene, we divided it as Cluster I, Cluster II, and Cluster III. Since most of the breakpoints were observed at Cluster II, it was chosen further in our study.

In the present study we report that Cluster II of breakpoint region of BCL6 5′UTR observed in DLBCL patients can fold into multiple non-B DNA structures such as hairpin DNA, triplex DNA and G4 DNA within the genome. We characterize each non-B DNA using in silico, biochemical and biophysical assays and demonstrate precise base pairing. Further we show that the formation of such structures could contribute towards replication arrest within the cells. Finally, we conclude that the single-stranded regions generated due to the formation of these structures may become an active site for action of enzymes such as AID, which was reported before in mature B cells.

Results

Mapping of DLBCL patient break points at 5′UTR of *BCL6* gene

Owing to the frequent translocation of *BCL6* with its 26 partner chromosomes (Fig. S1A), the translocation breakpoints associated with DLBCL patients were mapped on the genomic DNA sequence of the *BCL6* gene based on the information available from published studies and databases [6, 7, 10, 13, 15, 25, 33, 52, 53, 57, 60, 61]. We observed clustering of breakpoints at a 4 Kb region spanning the 5′UTR of the *BCL6* gene (Fig. S1B). Based on the distribution of breakpoints, we observed three peaks where most of the breakpoints were clustered, designated as Cluster I, Cluster II and Cluster III (Fig. S1B). All the three clusters are part of *BCL6* intron 1. Cluster I, II and III used in our study overlaps with the MTC while Cluster I overlaps with the MMC which is at the first exon–intron boundary. Since most of the breakpoints were seen at Cluster II, it was selected for further studies (Fig. 1A). However, the distribution was based on the ease of study and does not have any additional biological significance.

One of the primary reasons behind genomic instability in leukemia and lymphoma is the occurrence of non-B DNA structures [35, 46]. Based on previous studies from our laboratory and other groups, we hypothesised that the fragility of the Cluster II sequence of BCL*6* 5′UTR could be due to the formation of higher order DNA structures. Towards this, sequence from all three clusters were analyzed for non-B DNA sequence motifs using non-B DB v2.0 [5] (Fig. S1C). Interestingly, Cluster II showed the presence of mirror and inverted repeat sequence motifs. While inverted and mirror-repeat sequence was present in Cluster I, G4-forming motif was present in Cluster III (Fig. 1A; Fig. S1C). Further evaluation using mfold [63] revealed presence of 2 inverted repeat sequence motif in Cluster II (Fig. 1B; Fig. S1D). Inverted repeats can fold into hairpin structures, when present on single-stranded DNA or cruciform structures, when present on double-stranded DNA.

Electromobility shift assay reveal the formation of cruciform DNA at *BCL6* cluster II breakpoint region

Based on the "mfold web server" analysis, we investigated whether oligomeric DNA derived from *BCL6* cluster II breakpoint region (KDB7 and KDB8) could fold into hairpin structures (Fig. 1B, C). Towards this, oligomeric DNA sequence corresponding to the region of interest and its corresponding mutants were designed (Fig. 1C). The formation of hairpin structure would cause a difference in mobility when analyzed on a native PAGE as compared to a DNA sequence of the same length that does not form such a structure [18]. The radiolabelled oligomers were incubated in the presence of sodium cacodylate (20 mM), heat denatured at 95 °C, and then allowed to gradually cool to facilitate the structure formation. We observed a shift in mobility of wild-type oligomers (KDB7, KDB8 and KDB9) when compared with random controls (SCR239 and SS54) (Fig. 1D), indicating the formation of hairpin structures in wild-type oligomers. The oligomer KDB9, which harbors both the hairpin motifs, could potentially fold into a stem-loop structure (Fig. 1B, F). On the other hand, introduction of mutations in the cruciform forming sequence to abrogate the formation of cruciform structure (KDB10 and KDB11) showed mobility equivalent to that of normal single-stranded DNA (SCR239) (Fig. 1D), highlighting the folding of the inverted repeat sequences into stem-loop structure. Thus, our results indicate the formation of potential hairpin structures at *BCL6* cluster II region.

Circular dichroism studies reveal spectra characteristic of hairpin structures at *BCL6* cluster II region

CD studies were performed as described before [18]. CD studies are conducted on optically active molecules, in which the difference in the extent of polarization and that of absorption, can be estimated. Secondary structures of nucleic acids are known to impart a spectral pattern, distinct from that of B form of DNA. Thus, the oligomers derived from the *BCL6* cluster II region that could potentially form hairpin structures were subjected to CD spectroscopy (Fig. 1C). The wild-type oligomers, KDB7, and KDB8 showed a characteristic peak at 260–280 nm and dip at 240 nm while the mutant oligomers (KDB10 and KDB11), showed spectra similar to that of normal single-stranded DNA, with a positive peak at 280 nm and negative peak at 245 nm (Fig. 1E). Thus, the wild-type sequence derived from *BCL6* cluster II showed spectra characteristic of hairpin structures, which further indicates the formation of stem-loop structures in the wild-type oligomers KDB7, KDB8, and KDB9 (Fig. 1F).

Enzymatic and chemical probing confirm the formation of hairpin structure

P1 and S1 nucleases are specific to single-stranded DNA and can hydrolyse single-stranded region in duplex DNA such as loops or gaps. Since the proposed structure is a hairpin, it is expected to have a loop region that can be cleaved by

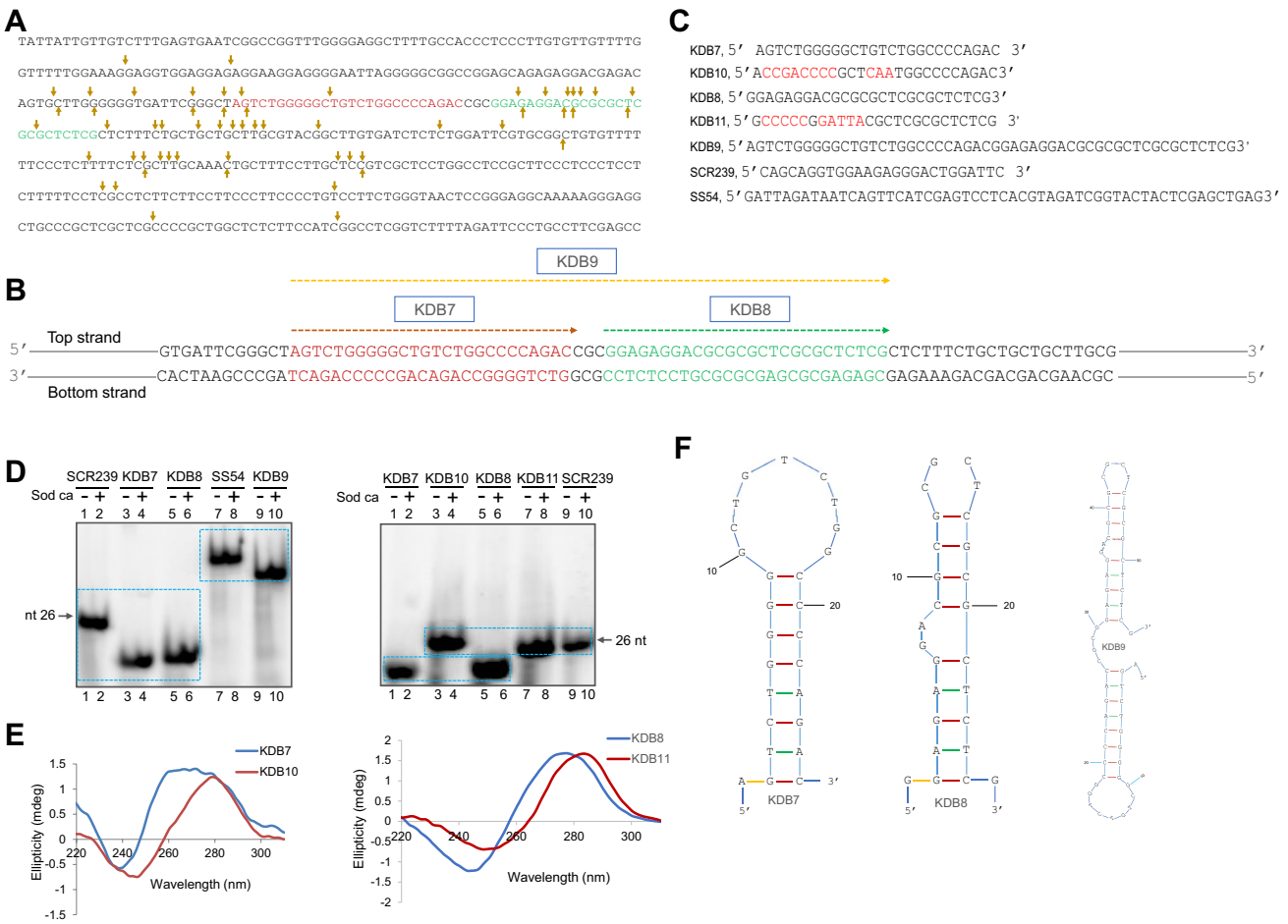

Fig. 1 Evaluation of the formation of hairpin DNA structures at cluster II of DLBCL patient breakpoint region at 5′UTR of *BCL6* gene. **A** To map the DLBCL patient breakpoints at *BCL6* gene, a portion of the human chromosome 3 genomic contig, GRch37.p13 Primary Assembly (NCBI Reference Sequence: NT_005612.16) sequence was retrieved from NCBI gene database using NCBI human genome map viewer. The sequences from the patients carrying translocation based on previous studies [6, 7, 10, 13, 15, 25, 33, 52, 53, 57, 60, 61] were analyzed using NCBI nucleotide BLAST, against *BCL6* sequence retrieved from NCBI database. Breakpoint regions identified in *BCL6* Cluster II region were then plotted and indicated using arrows. The inverted repeat sequences are highlighted in maroon and green colour, respectively. A breakpoint reported in top strand is indicated by downwards arrow, while upward arrow indicates a break at bottom strand. **B** Schematic representation of the position of hairpin-forming motifs (named as KDB7 and KDB8) of *BCL6* cluster II, as predicted by non-B DB v2.0. KDB9 is the sequence of KDB7 and KDB8 taken together. **C** Sequence of oligomeric DNA from cluster II region of *BCL6* used for the detection of cruciform structure using gel shift and circular dichroism assay. Sequence of oligomers KDB7, KDB8 and KDB9 (wild-type sequence), KDB10, KDB11 (mutants), SS54 and SCR239 (random sequence control) are also shown. Sequence highlighted in red indicate mutated nucleotides. **D** Radiolabelled oligomeric DNA were resolved on 15% native PAGE following incubation with 20 mM sodium cacodylate (Sod ca). Mobility of wild-type oligomers were compared with either random oligomers of equal length (SCR239 and SS54) or its mutants (KDB10 and KDB11). Both gel and buffer contain 1 M sodium cacodylate. The boxed region (blue) indicates substrates with different mobilities when run on a gel. **E** CD analysis of *BCL6* cluster II hairpin-forming oligomers and their mutants. CD spectra of wild-type oligomers KDB7 and KDB8 and their mutants KDB10 and KDB11 was recorded using JASCO J-810 spectropolarimeter with a scan range of 220 to 300 nm after incubating the oligomers in the presence of 20 mM sodium cacodylate, 100 mM NaCl, 0.1 mM EDTA at 37 °C for 1 h. **F** Predicted hairpin structures at *BCL6* cluster II (KDB7, KDB8 and KDB9) drawn using "mfold" analysis

single-stranded nucleases. To test this, 5′-end labelled oligomeric DNA of interest (wild-type, mutant, and random oligomers) were incubated with increasing concentrations of P1 nuclease (0.001, 0.01, 0.1, 0.5 U) and S1 nuclease (0.001, 0.01, 0.1, 0.5 U). Results from P1 nuclease assay revealed specific cleavage in the loop region of wild-type hairpin-forming oligomers (KDB7, KDB8, and KDB9) at higher nuclease concentrations, whereas mutant oligomers (KDB10 and KDB11) and random oligomer KDB9 showed random non-specific cleavage at the same concentration (Fig. 2A, C–E, H). Treatment with increasing concentrations of S1 nuclease also revealed a cleavage pattern consistent with hairpin DNA formation in the oligomers KDB7, KDB8, and KDB9 unlike random non-specific cleavage observed in

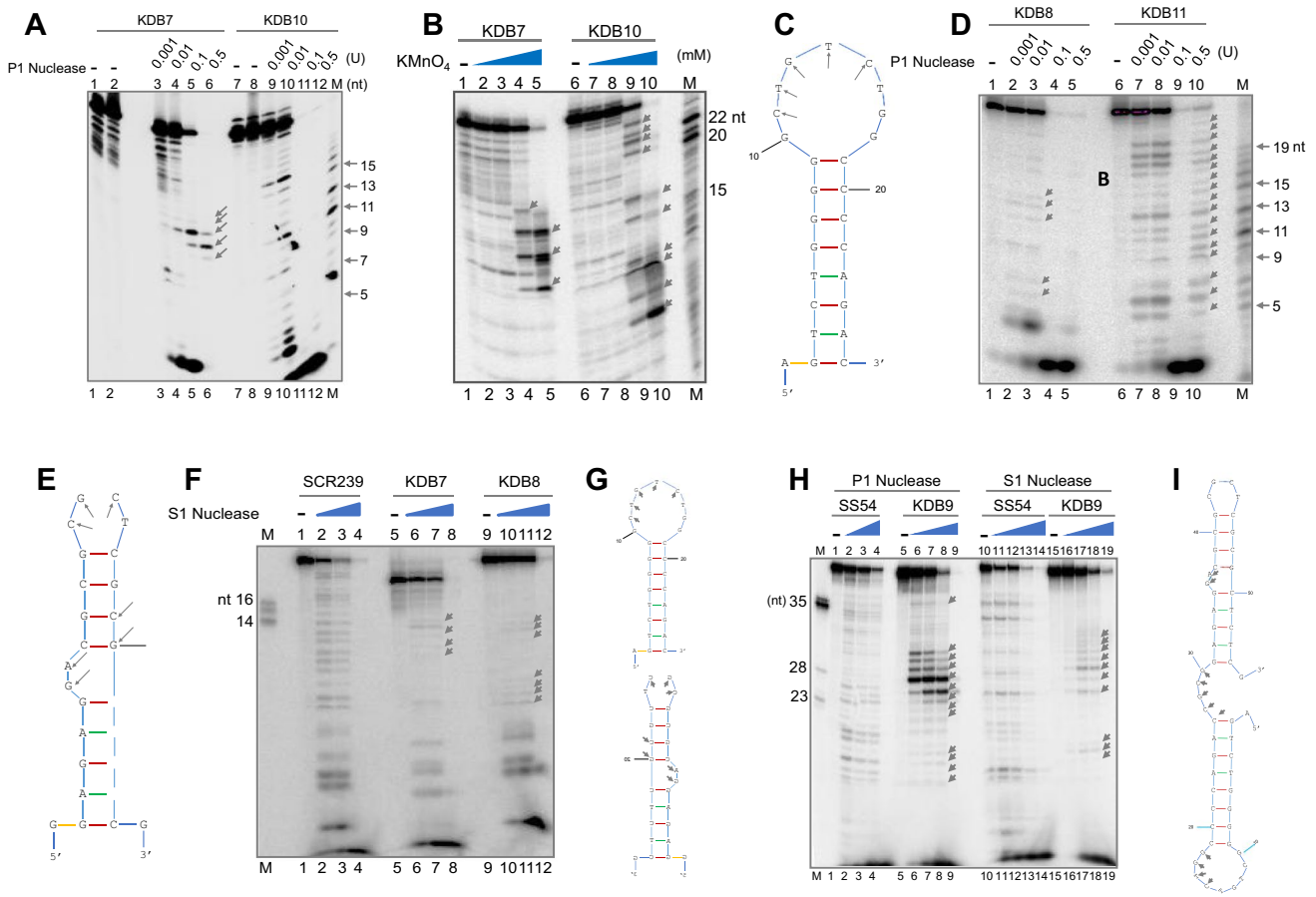

Fig. 2 Investigation of precise base pairing and single-strandedness based on enzymatic and chemical probing at cluster II region of *BCL6*. **A** Hairpin-forming oligomers from cluster II of *BCL6* 5′UTR, KDB7 (lanes 1–6) and its respective mutant KDB10 (lanes 7–12) were treated with increasing concentrations of P1 nuclease (0.001, 0.01, 0.1 and 0.5 U). **B** Oligomers from *BCL6* cluster II, KDB7 (lanes 1–5) and its mutant KDB10 (lanes 6–10) were treated with increasing concentrations of $KMnO_4$ (0.01, 0.1, 1 and 10 mM) and products were resolved on denaturing PAGE. **C** Stem-loop structure of KDB7 based on specific cleavage sites indicated with arrows in the putative structure. **D** Hairpin-forming oligomers from cluster II of *BCL6* 5′UTR, KDB8 (lanes 1–5) and its respective mutant KDB11 (lanes 6–10) were treated with increasing concentrations of P1 nuclease (0.001, 0.01, 0.1 and 0.5 U). **E** Stem-loop structure of KDB8 with the resulting specific cleavage sites indicated with arrows in the putative structure after digestion with P1 nuclease. **F** KDB7, KDB8 and random oligomer (SCR239) were treated with increasing concentrations of S1 nuclease (0.001, 0.01, 0.1 and 0.5 U). **G** Stem-loop structure of KDB7 and KDB8 with the resulting specific cleavage sites indicated with arrows in the putative structure based on digestion with S1 nuclease. **H** KDB9 treated with increasing concentrations of P1 nuclease (0.001, 0.01, 0.1 and 0.5 U) (Lanes 5–9) and S1 nuclease (Lanes 15–19) along with its random oligomer control SS54 (Lanes 1–4 and Lanes 10–14). **I** Stem-loop structure of KDB9 with the resulting specific cleavage sites indicated with arrows in the putative structure after digestion with P1/ S1 nuclease. In all the panels showing gel images, products were resolved on 15% denaturing polyacrylamide gels. Specific cleavage sites are indicated with arrows in the gel. 'M' represents marker

control oligomers (SCR239 and SS54) or mutant sequences (Fig. 2F–I). However, at times we have noted cleavage at certain nucleotides near the loop region, which could be due to presence of adjacent single-stranded regions.

$KMnO_4$ oxidizes unpaired thymine in the DNA (and to a lesser extent cytosines), which is then cleaved by piperidine. At appropriate concentrations of $KMnO_4$, the thymines present in the loop region of the hairpin are expected to be sensitive, while thymines in the double-stranded region are protected from $KMnO_4$ mediated oxidation. With increasing concentrations of $KMnO_4$ (0.01, 0.1, 1, and 10 mM), we observed specific cleavage mostly at thymine and to a lesser extent at cytosines, corresponding to the loop region of the oligomers, but not at the double-stranded stem region, confirming hairpin structure formation in KDB7 and KDB9 (Fig. 2B; Fig. S2A). The nucleotides that were present in the loop region of the wild-type oligomers were sensitive to KMnO4 while the stem region was protected (Fig. 2B; Fig. S2A, B). On the other hand, non-specific cleavage was observed for mutant (KDB10) as well as random oligomers (SB1), indicating absence of any secondary hairpin structures (Fig. 2B, Fig. S2A, C).

Non-B DNA structures formed at *BCL6* cluster II breakpoint region can block DNA replication

To study if hairpin/cruciform structure formation on a double-stranded DNA can prevent the progression of DNA polymerase during replication, 491 bp *BCL6* cluster II region was cloned into a plasmid to generate pKDB6 and was subjected to primer extension assay (Fig. 3A) as described before [22]. During primer extension, upon denaturation, the primer binds to one of the strands of the plasmid DNA, where the progression of polymerase is blocked due to the formation of non-B DNA structures (Fig. 3A). Radiolabeled primers positioned differentially from *BCL6* cluster II were used for primer extension studies (Fig. 3A). Interestingly, truncated primer extension products were seen due to premature pausing at the region of structure formation. Repositioning of the primer sequence showed a proportional change in the mobility of the pause sites. Interestingly, the positions of

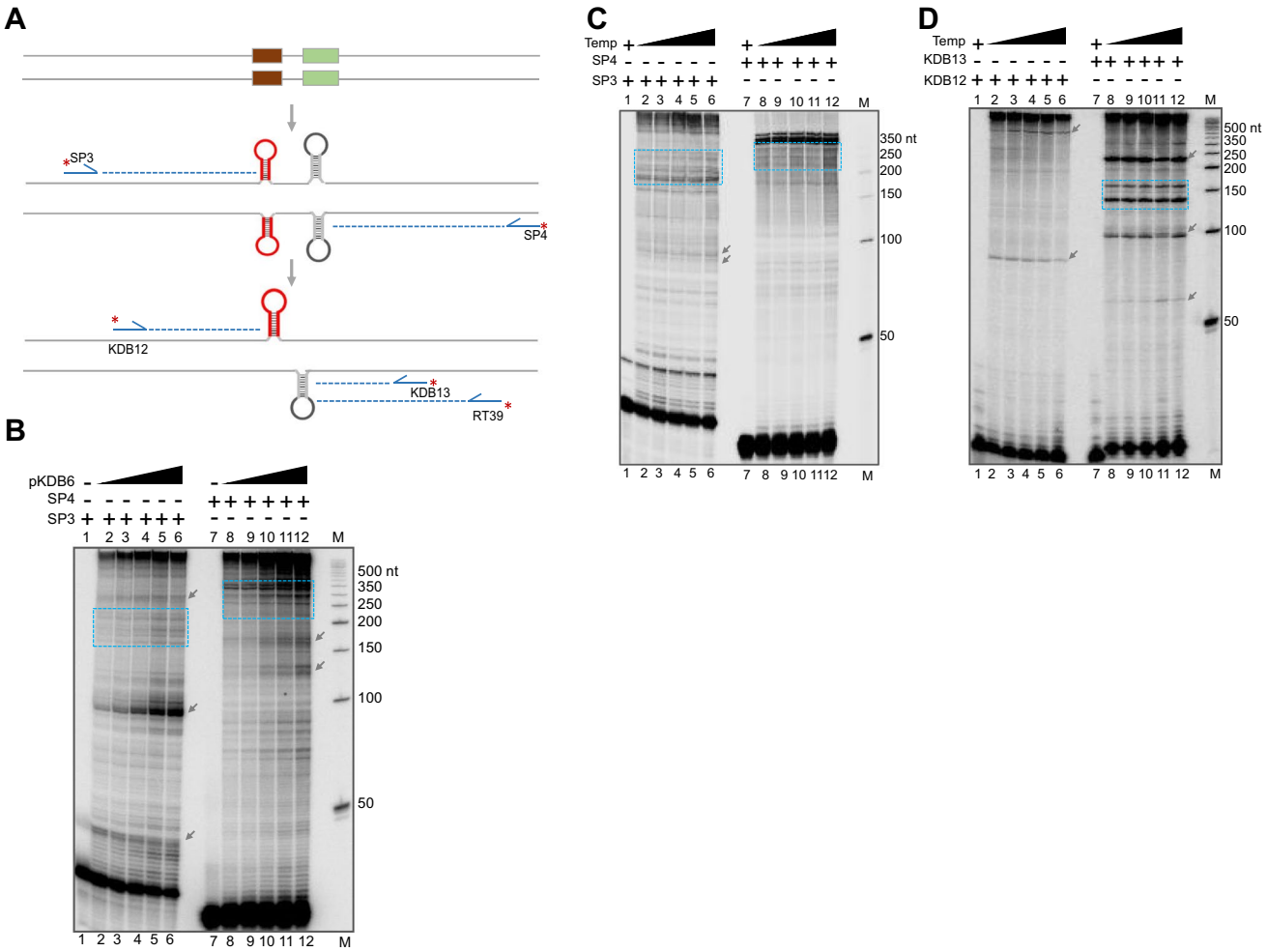

Fig. 3 Evaluation of DNA replication arrest due to the formation of non-B DNA structures at *BCL6* cluster II break point region, when present on a plasmid DNA using primer extension assay. **A** Schematic representation depicting primer extension strategy used for detecting the pause sites due to presence of non-B DNA structures. Upon denaturation, primer binds to one of the strands of the plasmid DNA where the progression of polymerase is hindered if non-B DNA structures are present. Differentially positioned radiolabeled forward (SP3* and KDB12*) and reverse primers (SP4*, KDB13* and RT39*) may hinder the progression of polymerase upon encountering hairpin structure on either strand, thereby causing a pause, which can be detected by electrophoresis on a denaturing gel. Sequence responsible for non-B DNA is represented as colored boxes, and hairpin formation upon denaturation is also indicated. **B**, **C** Primer extension on pKDB6 harboring *BCL6* cluster II (491 bp) using radio labelled primers, SP3 (Forward) and SP4 (Reverse) with increasing concentrations of plasmid (lanes 2, 8: 10 ng; 3, 9: 20 ng; 4, 10: 50 ng; 5, 11: 100 ng; 6, 12: 200 ng) (**B**), and at different annealing temperatures (Lanes 2, 8: 55 °C; 3, 9: 56.9 °C: 4, 10: 58.7 °C; 5, 11: 61.1 °C; 6, 12: 63 °C) (**C**). Lane 1 is SP3 alone and lane 7 is SP4 alone. **D** Primer extension of pKDB6 plasmid using KDB12 (Forward) and KDB13 (Reverse) primers with different annealing temperatures (Lanes 2,8: 55 °C; 3,9: 57.7 °C; 4,10: 60.2 °C; 5,11: 63.5 °C; 6,12: 67.9 °C). Lane 1 is KDB12 alone and lane 7 is KDB13 alone. Arrows show the pause sites at other regions and brackets indicate the pause sites due to the formation of hairpin/cruciform structure. For panel 'B–D', 'M' denotes 50 bp ladder. Pause sites of interest are either boxed (blue) or indicated by arrow

pauses due to polymerase arrest coincided with the region that is expected to form cruciform DNA (boxed in blue) when SP3, SP4, KDB12, KDB13, and RT39 primers were used (Fig. 3B–D). Increasing plasmid concentration (10, 20, 50, 100 and 200 ng) also led to an increase in the primer extension products corresponding to polymerase pause sites (Fig. 3B) although increase in temperature did not affect the intensity of pausing (Fig. 3C, D and data not shown). These results indicate that a hairpin/cruciform structure formation could block the progression of DNA polymerases, thus acting as a roadblock during DNA replication, at cluster II of *BCL6* breakpoint region. Interestingly, we have also observed pauses at places other than the expected regions (Fig. 3B–D), suggesting the possibility of the formation of other non-B DNA structures at *BCL6* cluster II region, which has been investigated in detail in this study (see below).

Bisulfite reactivity at *BCL6* cluster II suggests single-strandedness at the genomic loci in regions corresponding to different non-B DNA forming motifs

To investigate whether the region corresponding to *BCL6* cluster II possesses the single-strandedness in the genome, chromosomal DNA was isolated from REH and SUDHL8 cell line using nondenaturing method. Sodium bisulfite reacts with unpaired cytosines present on the complementary cytosine-rich strand and deaminates it to uracil, which upon PCR amplification and sequencing is read as thymine (Fig. 4A, B).

The inverted repeats sequences are present in both the top and bottom strand. 8 molecules from top strand and 15 from bottom strand showed C>T conversions in stretches (5 out of 8 molecules in the top strand shows conversion of six cytosines at a stretch and 7 out of 15 molecules shows conversion of nine cytosines at a stretch) in the *BCL6* cluster II breakpoint region corresponding to the cruciform forming sequence (Fig. 4C–E) suggesting single-strandedness of this region in the genome. Further analysis revealed that the additional regions of single-strandedness matched with pause sites observed during primer extension assay, indicating the possibility of the formation of other non-B DNA structures (G4 and triplex) at the cluster II of *BCL6* fragile region (Fig. 4C, E). Based on the bisulfite peaks and the additional pause sites observed during primer extension assay, we analyzed these additional single-stranded regions in *BCL6* cluster II for other non-B DNA sequence motifs at the 5′ end of cruciform forming motif (Fig. 4C). We found that there is a G-rich region just upstream to the cruciform forming region, that has the potential to form Hoogsteen hydrogen-base pairing with each other. Interestingly, the same region had most of the patient break points as well (Fig. S4). In addition, at the 5′ end of the cruciform forming region there is a mirror-repeat sequence that suggested the possibility of triplex formation. The formation of G-quadruplex and triplex structures at the above-mentioned regions were then investigated further.

G-rich template at *BCL6* cluster II breakpoint region forms G-quadruplex structure

Sodium bisulfite assay revealed that regions corresponding to the G4 motif possesses single-strandedness. To test whether the 'G'-rich strand can indeed fold into G-quadruplex structure, we designed oligomeric DNA corresponding to the region of interest, representing either the G-rich strand (VG3), C-rich complementary strand (VG4) or its mutants, where three (VG15), six (VG16), nine (VG17), and twelve (VG18) Gs were mutated in the wild-type sequence (VG3) (Fig. 5A). VG19 has one G of the GNG motif mutated to thymine (Fig. 5A). The formation of a G4 structure leads to a shift in the mobility as compared to a DNA sequence that does not form any structure, when analyzed on a native PAGE. To investigate this, radiolabeled oligomers were incubated in the presence or absence of KCl (100 mM), which is known to stabilize G-quadruplexes and the products were resolved on a 15% native PAGE with or without KCl in the gel and running buffer (Fig. 5B–D). Result showed that both C-rich and G-rich strands migrated according to the molecular weight in the absence of KCl (Fig. 5B, C). However, in the presence of KCl, we observed higher molecular weight bands for G-rich oligomer, which could be due to the formation of inter-molecular G-quadruplex structures (Fig. 5B, D). Importantly, we observed G-rich strand migrating faster than C-rich strand when K^+ was added in the reaction and gel (Fig. 5B, D). The faster moving species could be due to the formation of compact intramolecular G-quadruplex structures. Further, when increasing concentrations of VG3 oligomer were incubated in the presence of K^+ and resolved on the gel with 100 mM KCl, we observed that the intensity of intra and intermolecular G4 structures increased with increasing concentrations of DNA (Fig. S3A).

While in the presence of K^+ in the gel, we observed the formation of faster migrating intra molecular G-quadruplexes in VG3 and VG19 (Fig. 5D, lanes 3, 4, 13 and 14) it was abrogated in rest of the mutants (Fig. 5D, lanes 5–12). As expected, no such structures were observed in the case of the complementary C strand, VG4 (Fig. 5D, lanes 1, 2). To check the effect of mutation in GNG sequence on G-quadruplex formation, the mutated oligomer (VG19) was electrophoresed as described before. However, we did not find any effect of the mutation on the formation of G-quadruplex structures (Fig. 5C, D lanes 13, 14) suggesting that GNG sequence is not required for G-quadruplex structure formation.

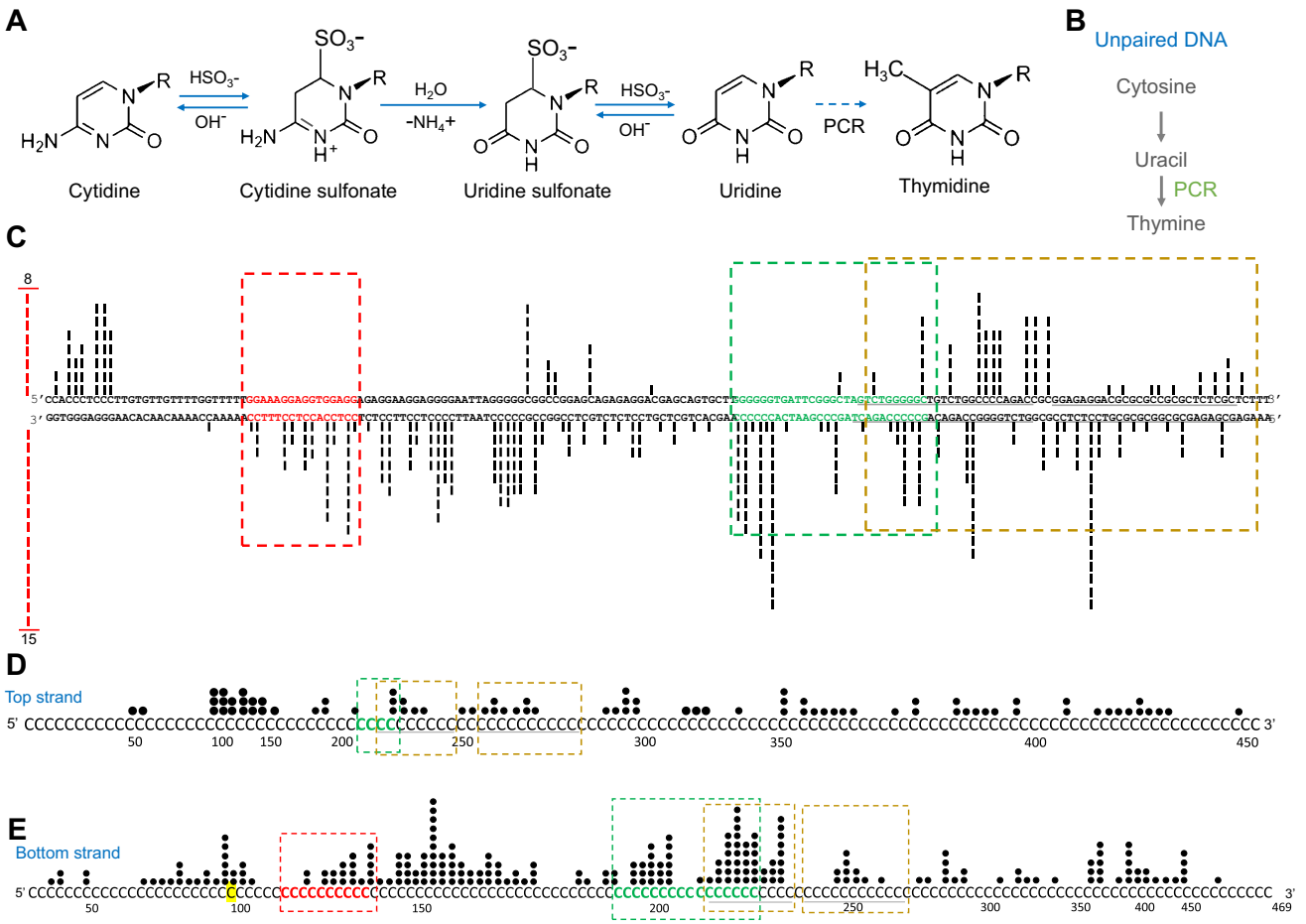

Fig. 4 Sodium bisulfite modification assay to determine single-strandedness at *BCL6* cluster II region in human genome. **A**, **B** Schematic representation of sodium bisulfite modification assay (**A**). Unpaired cytosine reacts with sodium bisulfite to give cytosine sulfonate, which upon deamination is converted to uracil sulfonate. Desulfonation of uracil sulfonate result in uracil, which following PCR is read as thymine (**B**). **C** Sodium bisulfite reactivity at the *BCL6* Cluster II gene when present on chromosomal DNA extracted from human DLBCL cells. The genomic DNA was extracted using non-denaturing conditions and subjected to sodium bisulfite modification assay. A 491 bp fragment corresponding to Cluster II was PCR amplified from chromosomal DNA after bisulfite treatment, cloned and sequenced. Vertical incremental bars above the cytosines represent the conversion of each cytosine to uracil in an individual molecule. The sequence corresponding to G-quadruplex region is marked in green, triplex region in red, hairpin in brown in both the top and bottom strand. The hairpin sequences are underlined, and the number of clones sequenced is indicated on the left. **D**, **E** Evaluation of extent of single-strandedness on top (**D**) and bottom strands (**E**) of *BCL6* cluster II, based on conversions seen in stretches as determined using sodium bisulfite assay. Cytosine to thymine conversion is indicated with filled circles, following bisulfite treatment in different molecules. *BCL6* cluster II sequence highlighted in red indicates triplex motif sequences. The sequence boxed in green indicates G-quadruplex and brown boxed region indicates cruciform forming motifs

It is known that K^+ stabilizes G-quadruplex structures while Li^+ does not [40]. The stability of the G-quadruplex structures in the presence of different cations was tested by incubating the G-rich oligomer in the presence of cations, K^+, Na^+, Li^+ and Ca^{2+}. The oligomers were then electrophoresed in 15% native PAGE in the presence of KCl (Fig. S3B). Results showed the formation of stable intramolecular G4 structures which was supported by presence of KCl in the gel, whereas intermolecular structures were seen more in the presence of K^+ (Fig. S3B, lanes 3, 4), followed by Na^+ (Fig. S3B, lanes 5, 6) and Ca^{2+} (Fig. S3B, lanes 9, 10). In the presence of Li^+, there were only few intermolecular species (Fig. S3B, lanes 7, 8), further confirming that the structure formation is supported maximally by monovalent cations, K^+ and Na^+. In the absence of KCl in the gel, we could observe only the formation of slower moving intermolecular species (Fig. S3C, lanes 1–10).

It has been shown that G-quadruplexes arrest the progression of DNA polymerases inside the cell [34]. To investigate the same, we performed Taq polymerase stop assay on an oligomeric single-stranded DNA derived from *BCL6* cluster II G-quadruplex forming region (VG20) and its mutant (VG23) (Fig. 5H). We found a major pause site in the wild-type of sequence, at 45 nt position, corresponding to the G-quadruplex

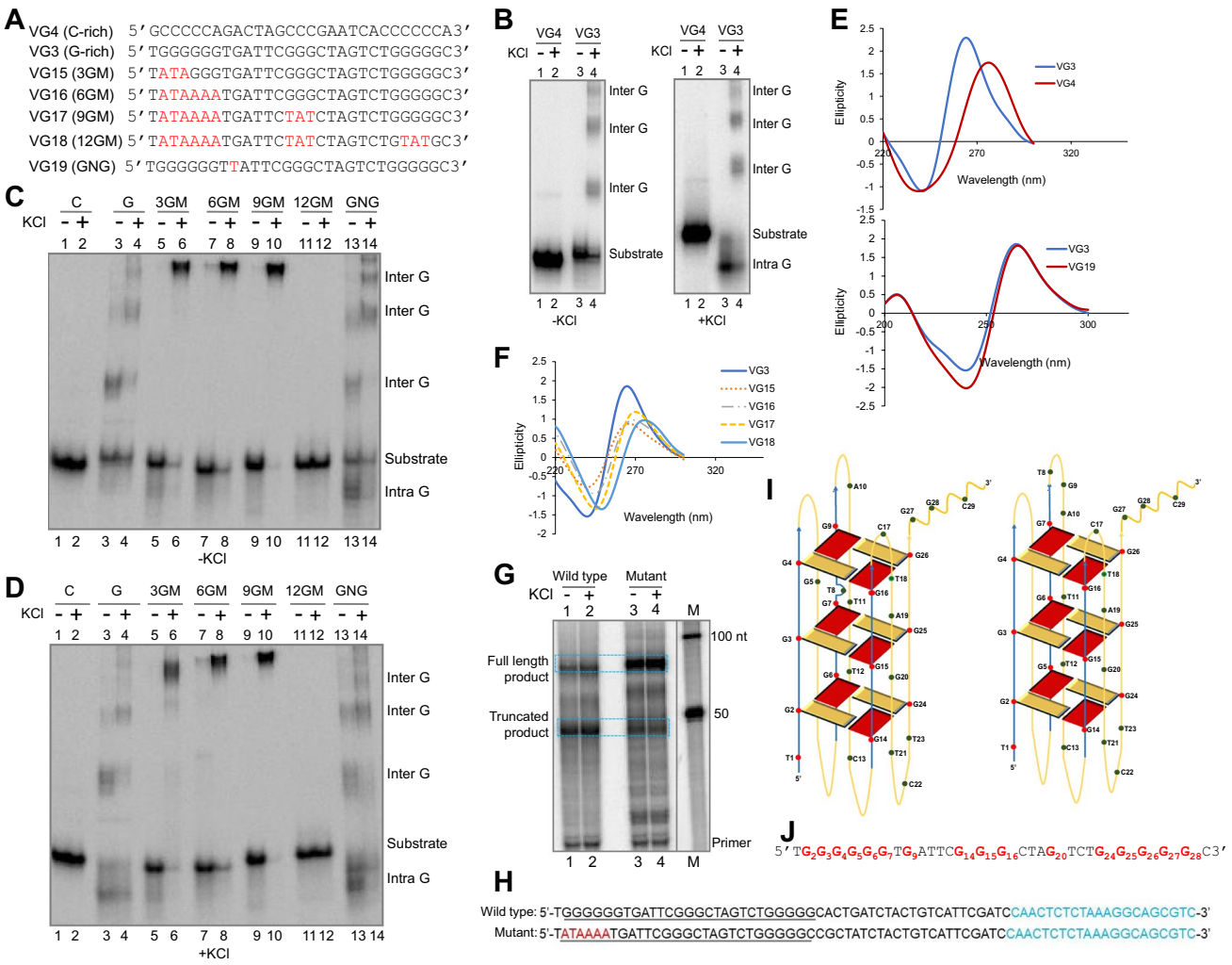

Fig. 5 Evaluation of G-quadruplex formation at *BCL6* cluster II. **A** Oligomeric DNA sequences spanning G-quadruplex forming region (VG3) and its complementary sequence (VG4) derived from *BCL6* cluster II. Mutations in G-rich strand was introduced such that three (VG15), six (VG16), nine (VG17), and twelve (VG18) guanine residues are changed to other nucleotides. In VG19, one guanine in the GNG motif is altered to thymine. **B**–**D** Evaluation of G-quadruplex formation by gel mobility shift assay at *BCL6* cluster. 'G' and 'C' rich sequences were incubated in 100 mM KCl at 37ºC for 1 h and resolved in the absence or presence of KCl in the gel and running buffer. Intramolecular (Intra G) and intermolecular (Inter G) quadruplex structures are indicated (**B**). Wild type and mutant oligomers were incubated either in the presence or absence of KCl (100 mM) and resolved on 15% native PAGE either in absence (**C**) or presence (**D**) of KCl in the gel and running buffer. Intramolecular (Intra G) and intermolecular (Inter G) quadruplex structures are indicated. **E**, **F** CD spectroscopy to determine G-quadruplex formation of 'G'-rich oligomers and their mutants. CD spectra of G-rich oligomer VG3, its complementary strand, VG4 and VG19, where one guanine of GNG motif is mutated (**E**). CD spectra of wild-type sequence (VG3) and mutants (VG15, VG16, VG17, VG18 and VG19) in presence of KCl (**F**). In both panels, the oligomers were incubated with 100 mM KCl and TE at 37 °C and CD spectra were recorded with the scan range of 220–300 nm. **G**, **H** Taq polymerase stop assay using oligomer sequence containing *BCL6* cluster II. The oligomers were heat denatured and gradually cooled in presence or absence of KCl (100 mM) along with Taq polymerase buffer and radiolabelled primer MN96 (**G**). M is 50 nt ladder. The truncated and full-length product is indicated on the gel. Sequence of G-quadruplex forming region in *BCL6* cluster II (VG20) and its mutant (VG23) (**H**). The first G-stretch mutated in VG23 is marked in red. Extra nucleotides are added at the 3′end, marked in blue, for primer binding. G-quadruplex forming region is underlined. **I** Representative 2D model of the two possible stable conformations of the intramolecular parallel G-quadruplex structure at the *BCL6* Cluster II. The position of guanines and other nucleotides involved are indicated. The strands are highlighted in blue and loops in yellow. Arrows indicate the orientation of the strands from 5′ to 3′ ends. **J** Sequence of the G-rich strand (VG3) from *BCL6* Cluster II where the guanines which are part of the three-plate G4 structure are highlighted in red

forming region (Fig. 5G, lanes 1, 2) which was less in the case of the mutant (Fig. 5G, lanes 3, 4). Consistent to this observation, the full-length product was abundant in the case of mutant compared to the wild-type of sequence (Fig. 5G). Thus, our result suggests that the formation of G-quadruplex

structures in *BCL6* cluster II region can halt the progression of polymerases and thus block DNA replication in the cell.

Circular dichroism studies reveal the formation of parallel G-quadruplex structure at *BCL6* cluster II region

To determine the orientation of G-quadruplex formed at *BCL6* cluster II, CD studies were carried out. The *BCL6* wild-type, mutant, and C-rich complementary oligomers were incubated in the presence of 100 mM KCl in TE at 37 °C for 1 h and CD spectra were recorded at RT. Results revealed that the G-rich strand, VG3, showed a peak around 265 nm and a dip at 240 nm, characteristic of a parallel form of G-quadruplex (Fig. 5E). Unlike the wild-type of oligomer (VG3), spectra derived from the mutant oligomers (VG15, VG16, VG17, and VG18) and the complementary C strand (VG4) showed a peak around 280 nm (Fig. 5E, F), resembling that of normal single-stranded DNA. However, when only one G of GNG is mutated (VG19), the spectra resembled ssDNA (Fig. 5E), suggesting no effect of this mutation on the G-quadruplex structure, further supporting the results obtained in EMSA.

Further, we performed CD studies of the G-rich oligomer in the presence and absence of KCl at increasing temperatures to determine whether the structure could be destroyed at higher temperatures (Fig. S3D-G). We observed that, in the presence of KCl, although at highest temperature (95 °C) there is slight decrease in the ellipticity, the structure was quite stable till 80 °C (Fig. S3D). In the absence of KCl, the spectra began to collapse slowly, indicating the instability of G4 DNA at higher temperatures (80 °C and 95 °C). However, even in the absence of KCl, the structure was stable till 65 °C (Fig. S3E). Gradual cooling of heat denatured (95 °C) sample to 25 °C in the presence of KCl restored the G4 structure (Fig. S3F) while such a phenomenon was not observed in the absence of KCl, even when the heat denatured (95 °C) sample was gradually cooled to 25 °C overnight (Fig. S3G). The formation of parallel G-quadruplex structure was shown to increase with increasing concentration of G-rich strand (Fig. S3H) further indicating that *BCL6* cluster II region can fold into an intramolecular parallel G-quadruplex structure. The guanine residues marked in the three-plate G4 structure renders stability to the structure while the other bases constitute the loop region (Fig. 5I, J). A representative 2D model demonstrating the formation of a parallel intramolecular G-quadruplex structure at the *BCL6* Cluster II region is presented (Fig. 5I).

Formation of triple-helical DNA structure at *BCL6* cluster II region

Since the bisulfite sensitive regions in *BCL6* cluster II region matched with a region corresponding to a mirror-repeat sequence, we have investigated the possibility of folding of these sequences into triple-helical DNA. The mirror-repeat containing oligomer VG10 has the ability to Watson–Crick base pair with the complementary strands, VG11 or VG12, and then fold onto itself by Hoogsteen hydrogen bonding resulting in a triplex DNA structure (Fig. 6A–C). Radiolabeled VG10 oligomer was incubated with increasing concentration of VG11 (0.1, 1, 10, 100, 500 nM) and VG12 (0.1, 1, 10, 100, 500 nM), resolved in 15% native PAGE, and evaluated for the formation of triplex DNA. A distinct shift in the mobility was observed at higher concentrations of VG11 (Fig. 6D, lanes 2–6) and VG12 (Fig. 6D, lanes 8–12), revealing a slower moving DNA species, which could be due to the formation of triplex DNA. The intermediate band seen could be due to duplex DNA between VG10 and complementary strand (Fig. 6D, lanes 2–4 and 8–10). To test the triplex DNA formation, oligomer VG10 was incubated with VG11 and VG12 in a buffer containing 90 mM Tris, 90 mM Borate and 10 mM $MgCl_2$ at 37 °C. CD spectroscopy was carried out over a wavelength range of 200–300 nm. CD spectra was also acquired with oligomers VG10 and VG11 alone and the spectra showed maximum molar ellipticity at a wavelength of 260 and 270 nm, respectively (Fig. 6E). When VG10 was added along with VG11 and VG12, a shift of the peak from 260 nm to 270–275 nm in the spectra was observed suggesting triplex formation (Fig. 6E).

Discussion

Multiple non-B DNA conformations in the cluster II region of *BCL6* gene

In the present study, we have investigated the mechanism that contributes to the fragility of cluster II of *BCL6* breakpoint region. Analysis of the breakpoint region in *BCL6* Cluster II revealed the presence of two inverted repeat sequence motifs that could fold into non-B DNA conformations. Previously, role of alternative DNA structures such as G-quadruplexes, triplexes and R-loops have been implicated in the generation of chromosomal translocations seen in follicular lymphoma, T-cell Leukemia and Burkitt's lymphoma etc. [19, 22, 34].

Using various biophysical and biochemical assays, we determined the formation of two independent hairpin DNA structures at the cluster II breakpoint region, which were abrogated upon mutation of the sequence. Using single-strand specific nucleases S1, P1 and $KMnO_4$ chemical probing, we determined the precise region of single-strandedness at the loop region confirming the formation of hairpin structure. When *BCL6* cluster II region was cloned into a plasmid to study the replication block due to the formation of cruciform DNA structure by primer extension assay, we observed

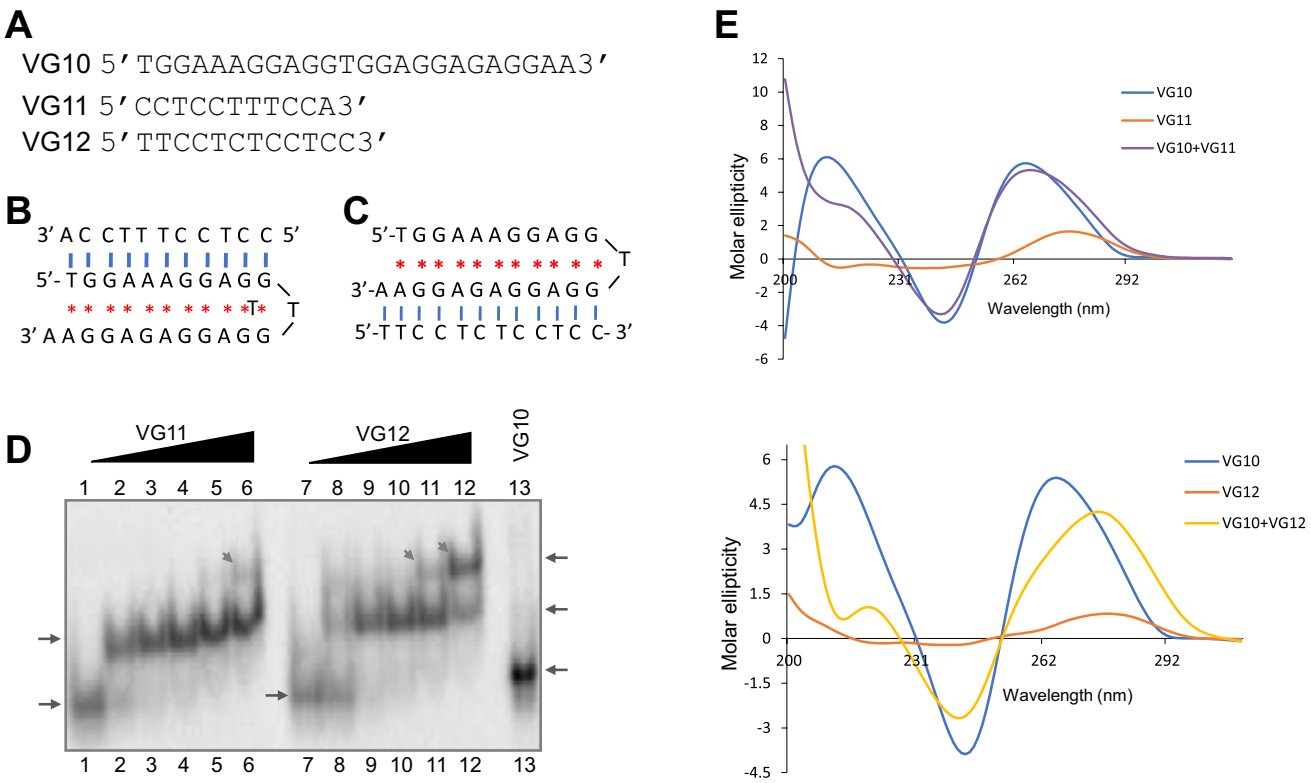

Fig. 6 Evaluation of triplex formation at *BCL6* cluster II. **A** Oligomers used for determination of triplex DNA formation at *BCL6* cluster II region. VG10 is the bottom strand which has the triplex forming motif derived from *BCL6* cluster II breakpoint region, and is complementary to pyrimidine rich oligomers, VG11 and VG12. **B**, **C** Schematic representation of the triple-helical structure in *BCL6* cluster II breakpoint region. '*' indicate Hoogsteen hydrogen bonding and blue vertical lines indicate Watson–Crick base pairing of VG10 with VG11 (**B**) or VG12 (**C**) are shown. **D** Gel shift assay to evaluate the formation of triplex DNA. VG10 was incubated with different concentrations of VG11 (Lanes 2–6) and VG12 (Lanes 8–12) and resolved on a 15% native PAGE with 1X Tris Borate and $MgCl_2$. Lanes 1 and 7 is VG10 alone and Lane 13 is heat denatured VG10. Bands of interest are shown by arrows. **E** CD studies to investigate triplex DNA formation at *BCL6* cluster II breakpoint region. CD spectra observed when VG10 (3 μM) was incubated along with VG11 (3 μM or 2 μM) or VG12 (3 μM or 2 μM). The incubation was done in presence of TBM buffer for 15 min at 37 °C. CD spectra were recorded at 25 °C where triplex forming oligos [(VG10 + VG11) and (VG10 + VG12)] showed positive peak at 280–290 nm different from normal B DNA peak at 260–280 nm

multiple pause sites accounting for other potential forms of DNA structures, besides the cruciform DNA. Consistent to this, we have observed multiple regions of single-strandedness in the genome when sodium bisulfite modification assay was used for investigation, which overlapped with patient breakpoint regions in cluster II.

The *BCL6* cluster II region could adopt a parallel intramolecular G-quadruplex structure and was dependent on K^+ for its formation and stability, which was abolished on mutating the G-stretch in the wild-type sequence, demonstrating the critical requirement of guanines during structure formation. When Taq polymerase stop assay was performed to evaluate the effect of G-quadruplex formation on DNA replication, we found pause sites matching with the region of G-quadruplex DNA, which was significantly reduced when mutant oligomers were used. This was also consistent with observed pause during primer extension in plasmids. In a similar manner using biochemical and biophysical assays, we determined the possibility of the formation of triplexes at *BCL6* cluster II. In summary, our studies reveal that multiple forms of higher order DNA structures may exist at *BCL6* cluster II breakpoint region contributing to the fragility of this region in the genome (Fig. 7; S4).

Non-B DNA structures and genomic instability

Depending on its sequence, physiological conditions, transcription, supercoiling stress etc., DNA has the ability to adopt different types of non-B DNA conformations [2, 35]. These non-B DNA structures are reported to be involved in a variety of biological functions. When the balance between replication, transcription and repair machinery is impaired, these secondary structures may induce genomic instability. Multiple studies have demonstrated DNA polymerase pausing in vitro and replication fork pausing in vivo owing to the structure formation [30, 34]. Several studies have pointed

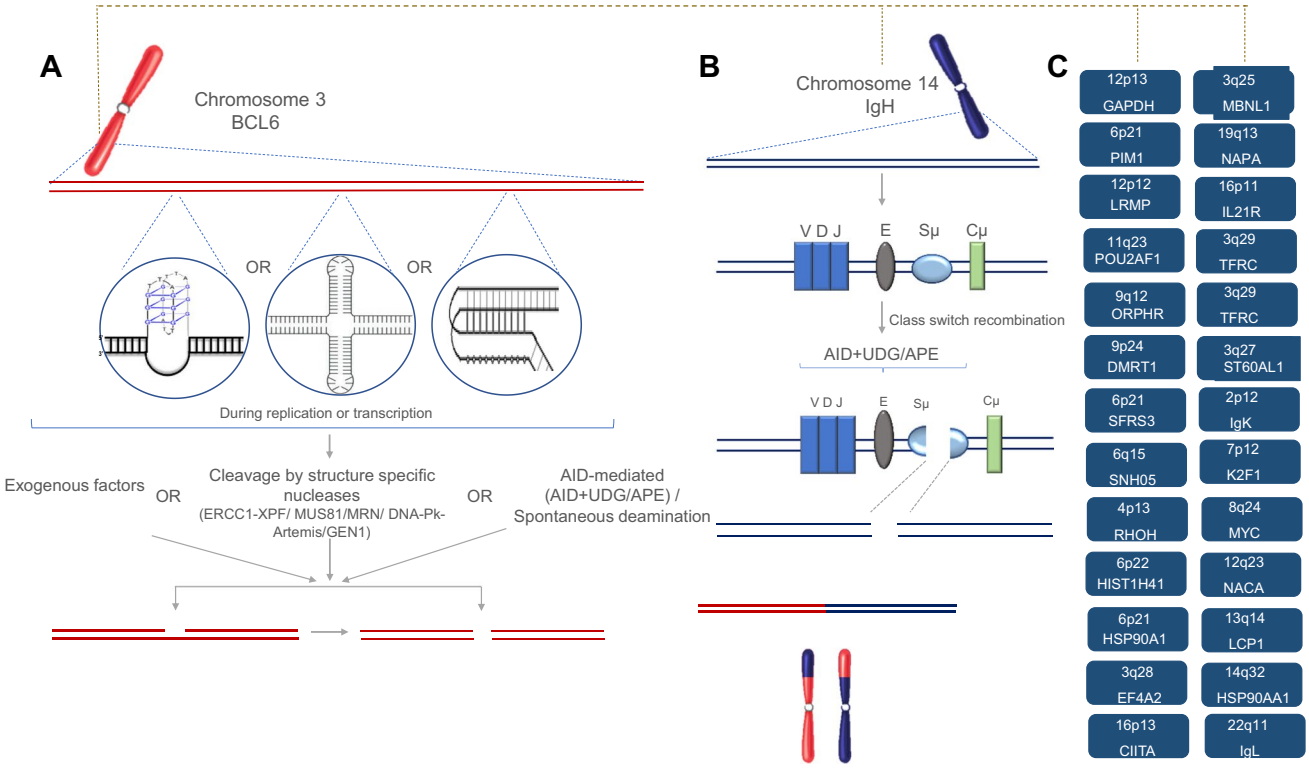

Fig. 7 A model depicting non-B DNA structure formation at the *BCL6* cluster II region and its role in *BCL6* translocations in DLBCL. The model illustrates one of the scenarios of *BCL6* translocation located in telomeric extremity, q arm of chromosome 3 (red) and IgH locus in chromosome 14 (blue), out of the 26 partner chromosomes it can pair with. During replication and transcription, local unwinding of the strands can lead to the formation of different non-B DNA structures at the *BCL6* cluster II region where break points are seen in patients. The formation of non-B DNA structures such as G4 DNA, triplex DNA or hairpin structure in one strand can lead to single-strandedness in the complementary strand, which are then prone to cleavage by nucleases like ERCC1-XPF, MUS81, MRN complex, DNA-Pk-Artemis, GEN1 etc. Spontaneous or AID-mediated deamination of cytosines can also occur in single-stranded region resulting in single-strand breaks. A nick generated by these nucleases during replication or transcription can lead to double-strand breaks. In the mature B cells, class switch recombination (CSR) occurs on chromosome 14 and AID plays a major role in CSR and SHM. Double-strand breaks occur at chromosome 14, due to interrupted CSR. These DSBs, if mis-repaired, can result in erroneous joining with another simultaneous break at *BCL6* gene, leading to the chromosomal translocation observed in DLBCL.

out the importance of altered DNA structures in the generation of DNA breaks and chromosomal translocations involved in cancer [37, 46].

Previous studies reveal that inverted repeat sequences often overlap with chromosomal regions prone to rearrangements [24] can be recognized and cleaved by endonucleases [26], and affect DNA replication of the region [1]. The formation of non-B DNA structures like G-quadruplex, triplexes, B/A transition, cruciform structures are reported at *BCL2* breakpoint region, that can lead to its fragility and potentiate chromosomal translocations [18, 35]. Some chromosomal translocations are reported due to inaccurate V(D)J recombination due to presence of cryptic RSS. RSS sequence are crucial for RAG cleavage and V(D)J recombination and presence of cryptic RSS sequence is often misrecognized by RAGs, undergo cleavage leading to double-strand breaks and subsequently chromosomal translocations [29, 45].

Triplexes can exist in chromosomes or nucleus and its formation in vivo is supported by a cohort of mammalian proteins that binds specifically to them [31]. Triplexes are also reported in human *c-MYC* promoter region which are shown to induce DSBs within these sequences and cause genomic instability in mice [3]. Resolvases like BLM and WRN can unwind triplexes and catalyze fork regression [4]. More recently DHX9, FANCJ are also reported to act as resolvases of triplexes [16, 49]. A recurrent non-Robertsonian translocation t(11;22) (q23;q11) in humans, specific to genome of human sperm, but not other somatic cells, was reported to harbor breakpoints in palindromic AT-rich repeats (PATRR) on 11q23 and 22q11 [23]. Formation of the cruciform structure has been related to disruption of MLL gene leading to generation of fusion proteins in both acute lymphoid and myeloid leukemias as well as translocations in Neurofibromatosis I [62]. The BCL2 major break point region, associated with the t(14;18) translocation in

follicular lymphoma, adopts a cruciform structure which possibly imparts single-strandedness to this region [18]. Thus, the formation of hairpin structure can lead to genomic rearrangements and translocations in different types of lymphoid cancer, if they are not resolved within the cells.

The RecQ family members like WRN and BLM are reported to unwind G-quadruplex DNA [12]. FANCJ is also reported to unwind G4 DNA [56]. Like triplexes, presence of G-quadruplex structures at the breakpoints of many genes, e.g., *BCL2*, *MYC, HOX11* etc. lead to gene rearrangements and translocations [18, 19]. The helicases that unwind such non-canonical DNA structures, also associate with several proteins critical for DNA replication and repair for the unhindered progression of replication forks [48]. Thus, mutation or deregulation of any of these proteins or enzymes will fail to destabilize these non-B DNA structures in the genome, thereby exposing them to nucleases like GEN1, MRN, DNA-PK Artemis, MUS81, ERCC1-XPF, and cytidine deaminase, AID, which act upon these fragile regions leading to DNA breaks (Fig. 7). The non-B DNA structures formed in the *BCL6* fragile region can get aberrantly cleaved by DNA repair proteins or nucleases resulting in double-strand breaks. Further, the presence of one structure can make immediate neighboring regions single-stranded, owing to the proximity of the sequence motifs, favoring the formation of other non-B DNA structures.

The formation of non-B DNA structures requires unwinding of double-stranded DNA, which occurs during the process of replication and transcription. Once a stable structure is formed at *BCL6* fragile region, it can be cleaved by nucleases at the single-stranded region creating a nick, which will subsequently result in double-strand break. Chromosomal translocations occur if there are simultaneous breaks in heterologous chromosomes. During class switch recombination (CSR) at the germinal center of mature B cells, AID acts upon single-stranded DNA in *IgH* locus leading to deamination of cytosines. Upon aberrant mismatch repair, it creates a nick in place of uracil, which eventually gets converted as a DSB. A break at the *BCL6* 5′ UTR during the same window places the *BCL6* gene under the promoter of *IgH* locus, thereby resulting in overexpression of *BCL6* (Fig. 7). However, this just explains one of the scenarios of *BCL6* translocation and as described above *BCL6* gene can fuse with 26 partner genes in different chromosomes studied in different DLBCL patients. The reason behind the breaks observed in other genes needs to be investigated further. One probable reason could be aberrant somatic hypermutation in B cells that targets many genes, including *BCL6.* The role of structure-specific nucleases and cytidine deaminases behind the generation of DSB in the region warrants further investigation.

In summary, we determine the formation of non-B DNA structures such as, G-quadruplex, cruciform and triplex DNA at the breakpoint region (Cluster II) of *BCL6* gene which may play a role in its fragility, due to its potential to fold into altered DNA structures. The formation of hairpin and G4 DNA together in Cluster II contributes to the fragility of *BCL6* gene. The non-B DNA structures like hairpin and G-quadruplex are formed in the genome of healthy individuals on unfolding of the respective non-B DNA motifs. In most cases, they are unwound by resolves and helicases inside the cells. When such structures are stably formed within the cells, endonucleases or deaminases may bind to it and lead to generation of DNA breaks or secondary mutations inside the cells. These processes subsequently promote translocation events in *BCL6* gene. However, only the translocations which lead to BCL6 overexpression will have pathological consequences since translocations are also present in healthy individuals [37]. Besides, the presence of gaps or breaks at Cluster I or Cluster III and non-B DNA sequence motifs could also lead to DNA double-strand breaks in these regions followed by *BCL6* gene translocation, which are under investigation.

Materials and methods

Enzymes, chemicals, and reagents

Chemical reagents were obtained from Sigma Chemical Co. (USA), SRL (India). Culture media were from Lonza (UK) and MP Biomedicals (USA). Fetal bovine serum (FBS) and PenStrep were purchased from Gibco BRL (USA), Restriction endonucleases and DNA-modifying enzymes were from New England Biolabs (Beverly, MA, USA). Radioisotope γ-^{32}P-ATP was from BRIT (India). Wizard DNA purification system was obtained from Promega (Madison, USA).

Oligomeric DNA

The sequence of DNA oligonucleotides used in the current study are listed (Table S1). Oligomers were designed and commercially synthesized by IDT (Coralville, IA, USA) and Juniper Life Sciences (Bangalore, India). The oligomers were purified using 8–18% denaturing PAGE as described before [21]. The gel piece with the oligomer was crushed and incubated in 500 mM NaCl in Tris–EDTA overnight at 37 °C, followed by phenol–chloroform extraction and precipitation. 5′ end labelling of oligomers was carried out using T4 Polynucleotide Kinase in a buffer containing 20 mM Tris acetate (pH 7.9), 10 mM Magnesium acetate, 50 mM Potassium acetate, 1 mM DTT and γP^{32} ATP, at 37ºC for 1 h. The labelled oligomers were then purified using G-25 Sephadex columns and stored at -20ºC till further use. To generate double-stranded oligomeric DNA,

complementary oligomers were annealed in 100 mM NaCl and 1 mM EDTA.

Cell lines and culture

Human diffuse large B cell lymphoma cell line SUDHL8 was a kind gift from Dr. A. Epstein, USA. Human B cell precursor leukemia cell line REH was from Dr. M.R. Lieber, USA. Cells were cultured in RPMI 1640 supplemented with 10% fetal bovine serum (FBS), 100 µg/ml Penicillin, and 100 µg/ml streptomycin and incubated at 37 °C in a humidified atmosphere containing 5% CO_2.

Plasmid constructs

pKDB6 was constructed by cloning the *BCL6* cluster II sequence, PCR amplified from human genomic DNA and cloned at the BamHI site of pMN4 [36] in physiological orientation. The cloned inserts were confirmed by DNA sequencing.

Preparation of Klenow ladder

The 5′ end labelled DNA was incubated in a buffer (10 mM Tris–HCl (pH 7.9), 10 mM $MgCl_2$, 150 mM NaCl and 1 mM DTT) with Klenow polymerase for partial digestion at room temperature for 1 h. The reaction was terminated by adding formamide containing dye. The reaction products were diluted and loaded on denaturing polyacrylamide gels.

Hairpin DNA formation

'Mfold' analysis showed that the top strand of *BCL6* cluster II region has the ability to form hairpin structures. Those sequences (KDB7, KDB8 and KDB9) were commercially synthesized and purified as described above. The sequences were then γ-^{32P}-ATP end labelled. The products were resolved on a 12% denaturing PAGE. The signals were detected after drying the gel using a phosphorImager.

Analysis of triplex DNA

The radiolabeled oligomer VG10 was incubated with increasing concentrations of VG11 (0.1, 1, 10, 100, 500 nM) and VG12 (0.1, 1, 10, 100, 500 nM), and evaluated for the formation of triplex DNA in 90 mM Tris, 90 mM Borate and 10 mM $MgCl_2$ (pH 8.0) at 37 °C overnight. The products were then resolved on 15% native polyacrylamide gels at 150 V at 4 °C [21]. The gels were dried and exposed to a screen, and the signal was detected using phosphorImager FLA9000 (Fuji, Japan).

G4 DNA formation

The radiolabeled oligomers with G4 motifs and their corresponding mutants were incubated either in the presence or absence of 100 mM KCl in TE buffer (pH 8.0) at 37 °C for 1 h. The oligomers were then resolved on 15% native polyacrylamide gels in the presence or absence of 100 mM KCl, both in the gel and the buffer, at 150 V at room temperature. The gels were dried and exposed to a screen, and the signal was detected using phosphorImager FLA9000 (Fuji, Japan).

Electrophoretic mobility shift assay

The radiolabeled oligomers (wild-type and mutants) were incubated in the presence of 20 mM sodium cacodylate for hairpin/cruciform structure forming oligos, 10 pM–100 mM KCl for G-quadruplex forming oligomeric DNA and Tris–borate buffer (90 mM Tris, 90 mM Boric acid and 10 mM $MgCl_2$) for triplex DNA. The products were then resolved on 12–15% native polyacrylamide gels at 150 V at RT. The G-quadruplex forming oligomers were resolved in the presence or absence of 100 mM KCl, both in the gel and the buffer. The gels were dried and exposed to a screen and the signal was detected using phosphorImager FLA9000.

Circular dichroism (CD) spectroscopy

The wild-type and mutant oligomers for hairpin/cruciform structure from *BCL6* 5′UTR were incubated in the presence of 20 mM sodium cacodylate, 100 mM NaCl, 0.1 mM EDTA at 37 °C for 1 h [36]. G-quadruplex forming oligomer, its mutants and the complementary oligomer were incubated either in the presence or absence of 100 mM KCl in TE at 37 °C for 1 h. Triplex forming oligomers were incubated with TBM buffer at same reaction conditions. The oligomer concentration used was 4 µM. The CD spectra was recorded at room temperature with a scan range of 220 to 300 nm and 5 cycles were accumulated for every sample, using JASCO J-810 spectropolarimeter at a scan speed of 50 nm per min. Separate spectrum was measured for the buffer alone and this was subtracted from all the experimental spectra.

For G-quadruplex oligomers, absorbance was measured in the absence of KCl to check the stability of the structure. For the dissolution of G4 structures, the spectra were recorded for the samples incubated with and without KCl at increasing temperatures (25–95 °C). Further CD spectrum was recorded after the structure was reformed by gradually cooling the denatured oligos to 25 °C. The ellipticity was calculated using the software, Spectra manager and plotted as a function of wavelength.

P1 nuclease assay

The P1 nuclease assay was performed as described earlier [32]. The 5′-end labelled oligomers containing inverted repeat sequence that is predicted to form hairpin structure from *BCL6* cluster II region, were incubated with different concentrations of P1 nuclease (0001, 0.01, 0.1, 0.5 U), for 30 min, at 37 °C in a buffer containing 50 mM NaCl, 10 mM Tris–HCl, 10 mM $MgCl_2$ and 1 mM DTT. The reaction was stopped by adding 20 mM EDTA and the products were resolved on 15% denaturing PAGE.

$KMnO_4$ probing assay

The radiolabeled oligomers from *BCL6* cluster II region, were denatured at 95 °C and then gradually cooled to allow the structure formation, followed by incubation in the presence of increasing concentration of $KMnO_4$ (0.01, 0.1, 1, 10 mM) for 30 min at room temperature. The reaction was stopped by addition of equal volume of stop buffer (50 mM EDTA, 1% SDS, 400 mM β-mercaptoethanol) [32]. The oligomers were further treated with equal volume of piperidine (10%) and incubated at 90 °C for 30 min. The reaction was diluted to double the volume and dried under vacuum. DNA was then washed and precipitated, and samples were electrophoresed on 15% denaturing PAGE to score for the cleaved sites.

Primer extension assay

The replication blocks caused due to the formation of non-B DNA structures at the 5′UTR of *BCL6* was studied on plasmid, pKDB6 harboring cluster II, using primer extension [8]. The reaction was carried out using radiolabeled primers (SP3, SP4, KDB12, KDB13, and RT39) and 50 ng plasmid with varying temperatures (50–65 °C). The reaction was also performed using different concentrations of plasmids (10–200 ng) at an optimum temperature selected for each primer. The reaction mix contains 1X Thermo polymerase buffer (10 mM KCl, 10 mM $(NH_4)_2SO_4$, 20 mM Tris–HCl (pH 8.8), 4 mM $MgSO_4$, and 0.1% Triton X-100), 200 µM dNTPs, 0.5 µM end labelled primers and 1 U vent (exo-) polymerase. Linear amplification by primer extensions were carried out on a PCR machine (25 cycles) under the following conditions: 95 °C for 3 min (1 cycle), 95 °C for 45 s, 50–65 °C for 45 s and 72 °C for 45 s and final extension of 3 min. The reactions were then terminated by adding formamide dye and products were resolved on 8% denaturing PAGE. The gel was dried, and signals were detected using phosphorImager FLA9000 as described above.

Taq polymerase stop assay

Taq polymerase stop assay was performed as described before with modifications [38]. The *BCL6* cluster II G-quadruplex forming oligomer, VG20 and its mutant VG23 were heat denatured and slowly reannealed in the presence or absence of KCl in buffer containing 10 mM Tris–HCl and 1.5 mM $MgCl_2$ and radiolabelled MN96. After addition of 200 µM dNTPs and 1 U Taq polymerase, the reactions were incubated at 55 °C for 30 min. The reaction was stopped by addition of 1X formamide dye and the products were resolved on 12% denaturing PAGE and visualised as described above.

Sodium bisulfite modification assay

Bisulfite modification was carried out as described previously [38]. 1 µg of genomic DNA, extracted from SUDHL8 cells under non-denaturing conditions, was resuspended in 30 µl of distilled water, mixed with 12.5 µl of 20 mM hydroquinone and 457.5 µl of 2.5 M sodium bisulfite (pH 5.2). The mixture was incubated for 16 h at 37 °C in the dark. The bisulfite-treated DNA was purified with the Wizard DNA clean-up kit (Promega) according to the manufacturer's instructions. Purified bisulfite-treated DNA was desulfonated with 0.3 M NaOH at 37 °C for 15 min. Desulfonated DNA was precipitated with 96 µl of 7.5 M NH_4OAc and 768 µl of Ethanol at -20 °C for > 2 h and washed with 70% ethanol and resuspended in TE (pH 8.0). PCR with bisulfite-modified DNA as a template was carried out with the primers RT38 and RT39. The PCR products were resolved on agarose gels and the correct sized fragment was recovered. Purified PCR products were cloned with TA cloning kit (Genei, Bangalore, India). Plasmid DNA was isolated from each clone using Alkaline Lysis Method. The sequencing of the clone was carried out at Medauxin, Bangalore, India.

Extraction of chromosomal DNA

Chromosomal DNA was isolated from REH (leukemia cells) and SUDHL8 cells (DLBCL cells) using non-denaturing method [38]. Briefly, SUDHL8 cells were collected by centrifugation and washed with 1X PBS, followed by extraction of chromosomal DNA by lysing the cells in TE (10 mM Tris (pH 8.0) and 1 mM EDTA) and 0.5% SDS. Chromosomal DNA was then digested overnight by incubating it with proteinase K (20 µg/ml) at 37 °C. The genomic DNA was phenol, phenol: chloroform (50:50) and chloroform extracted, followed by precipitation in chilled 100% ethanol. DNA was rinsed in 70% ethanol and air dried. The pellet was resuspended in TE.

Purification of plasmid DNA

Plasmid DNA was isolated from *E. coli* DH5α cells using nondenaturing method and purified by cesium chloride density gradient centrifugation. Briefly, 5.1 g CsCl was dissolved in 4.0 ml TE, followed by addition of 5–10 mg plasmid and ethidium bromide. Samples were centrifuged using TLA110 rotor (Beckman Coulter, USA) for 12 h, 72,000 rpm at 20 °C. Following butanol extraction for removal of ethidium bromide, the plasmid DNA was precipitated with chilled ethanol, washed in 70% alcohol, and pellet dissolved in Tris–EDTA buffer.

S1 nuclease assay

For the S1 nuclease assay wild-type oligomers KDB7, KDB8, and KDB9 and random oligomers SCR239 and SS54 were heat denatured at 95 °C and cooled overnight in a water bath. Oligomers were then treated with 0.001, 0.01, 0.1, and 0.5 U of S1 nuclease (Fermentas, USA) in a buffer containing 200 mM sodium acetate (pH 4.5 at 25 °C), 1.5 M NaCl, and 10 mM $ZnSO_4$ for 30 min at 37 °C, and the DNA was purified by phenol–chloroform extraction. The reaction products were resolved on a 15% denaturing PAGE and analyzed.

2-D modelling of G4 DNA

2-D modelling of G4 DNA formed at *BCL6* Cluster II was performed as described before [8]. The position of guanines and other nucleotides involved are indicated. The stacks are highlighted in red and yellow, and the loops in yellow. Arrows indicate the orientation of the strands @@@(Fig. 5I).

Supplementary Information The online version contains supplementary material available at https://doi.org/10.1007/s00018-023-05042-w.

Acknowledgements We thank Mr. Arun Sharma, Mr. Sayak Das and other members of the SCR laboratory for discussions and comments on the manuscript.

Author contributions SCR and BC conceived and coordinated the study; SCR, BC, and VG designed experiments; VG, UR, SS, KBD, SS, SMJ, and BC performed experiments; SCR, VG, UR, and BC interpreted the data and wrote the paper.

Funding This work was supported by grants from the Leukemia Research , USA (LRF/2010), Department of Biotechnology (DBT), India BT/PR13722/BRB/10/781/ 2010 for SCR and DAE, India (Grant No. 21/01/2016-BRNS/35074) to SCR. VG is supported by Senior Research Fellowship (SRF) from CSIR, India, and UR by SRF from IISc (Grant No. BT/PR27952-INF/22/212/2018).

Data availability The authors declare that the main data supporting the findings of this study are available within the article and its Supplementary Material.

Declarations

Conflict of interest Authors disclose that there is no conflict of interest.

References

1. Ahmed A, Podemski L (1998) Observations on template switching during DNA replication through long inverted repeats. Gene 223:187–194
2. Bacolla A, Wells RD (2009) Non-B DNA conformations as determinants of mutagenesis and human disease. Mol Carcinog 48:273–285
3. Belotserkovskii BP, Mirkin SM, Hanawalt PC (2013) DNA sequences that interfere with transcription: implications for genome function and stability. Chem Rev 113:8620–8637
4. Brosh RM Jr, Majumdar A, Desai S, Hickson ID, Bohr VA, Seidman MM (2001) Unwinding of a DNA triple helix by the Werner and Bloom syndrome helicases. J Biol Chem 276:3024–3030
5. Cer RZ, Donohue DE, Mudunuri US, Temiz NA, Loss MA, Starner NJ, Halusa GN, Volfovsky N, Yi M, Luke BT et al (2013) Non-B DB v2.0: a database of predicted non-B DNA-forming motifs and its associated tools. Nucleic Acids Res 41:D94-d100
6. Chaganti SR, Chen W, Parsa N, Offit K, Louie DC, Dalla-Favera R, Chaganti RS (1998) Involvement of BCL6 in chromosomal aberrations affecting band 3q27 in B-cell non-Hodgkin lymphoma. Genes Chromosom Cancer 23:323–327
7. Chaganti SR, Rao PH, Chen W, Dyomin V, Jhanwar SC, Parsa NZ, Dalla-Favera R, Chaganti RS (1998) Deregulation of BCL6 in non-Hodgkin lymphoma by insertion of IGH sequences in complex translocations involving band 3q27. Genes Chromosom Cancer 23:328–336
8. Dahal S, Siddiqua H, Sharma S, Babu RK, Rathore D, Sharma S, Raghavan SC (2022) Unleashing a novel function of Endonuclease G in mitochondrial genome instability. Elife 11:e69916
9. Del Mundo IMA, Zewail-Foote M, Kerwin SM, Vasquez KM (2017) Alternative DNA structure formation in the mutagenic human c-MYC promoter. Nucleic Acids Res 45:4929–4943
10. Fenton JA, Schuuring E, Barrans SL, Banham AH, Rollinson SJ, Morgan GJ, Jack AS, van Krieken JH, Kluin PM (2006) t(3;14)(p14;q32) results in aberrant expression of FOXP1 in a case of diffuse large B-cell lymphoma. Genes Chromosom Cancer 45:164–168
11. Frank-Kamenetskii MD, Mirkin SM (1995) Triplex DNA structures. Annu Rev Biochem 64:65–95
12. Fry M, Loeb LA (1999) Human werner syndrome DNA helicase unwinds tetrahelical structures of the fragile X syndrome repeat sequence d(CGG)n. J Biol Chem 274:12797–12802
13. Galiègue Zouitina S, Quief S, Hildebrand MP, Denis C, Lecocq G, Collyn-d'Hooghe M, Bastard C, Yuille M, Dyer MJ, Kerckaert JP (1996) The B cell transcriptional coactivator BOB1/OBF1 gene fuses to the LAZ3/BCL6 gene by t(3;11)(q27;q23.1) chromosomal translocation in a B cell leukemia line (Karpas 231). Leukemia 10:579–587
14. Gellert M, Lipsett MN, Davies DR (1962) Helix formation by guanylic acid. Proc Natl Acad Sci USA 48:2013–2018
15. Hosokawa Y, Maeda Y, Ichinohasama R, Miura I, Taniwaki M, Seto M (2000) The Ikaros gene, a central regulator of lymphoid

differentiation, fuses to the BCL6 gene as a result of t(3;7)(q27;p12) translocation in a patient with diffuse large B-cell lymphoma. Blood 95:2719–2721
16. Jain A, Bacolla A, Chakraborty P, Grosse F, Vasquez KM (2010) Human DHX9 helicase unwinds triple-helical DNA structures. Biochemistry 49:6992–6999
17. Jardin F, Ruminy P, Bastard C, Tilly H (2007) The BCL6 proto-oncogene: a leading role during germinal center development and lymphomagenesis. Parodontol 55:73–83
18. Javadekar SM, Yadav R, Raghavan SC (2018) DNA structural basis for fragility at peak III of BCL2 major breakpoint region associated with t(14;18) translocation. Biochim Biophys Acta 1862:649–659
19. Katapadi VK, Nambiar M, Raghavan SC (2012) Potential G-quadruplex formation at breakpoint regions of chromosomal translocations in cancer may explain their fragility. Genomics 100:72–80
20. Klein U, Dalla-Favera R (2008) Germinal centres: role in B-cell physiology and malignancy. Nat Rev Immunol 8:22–33
21. Kumari N, Vartak SV, Dahal S, Kumari S, Desai SS, Gopalakrishnan V, Choudhary B, Raghavan SC (2019) G-quadruplex structures contribute to differential radiosensitivity of the human genome. iScience 21:288–307
22. Kumari R, Nambiar M, Shanbagh S, Raghavan SC (2015) Detection of G-quadruplex DNA using primer extension as a tool. PLoS ONE 10:e0119722
23. Kurahashi H, Emanuel BS (2001) Long AT-rich palindromes and the constitutional t(11;22) breakpoint. Hum Mol Genet 10:2605–2617
24. Kurahashi H, Inagaki H, Ohye T, Kogo H, Kato T, Emanuel BS (2006) Palindrome-mediated chromosomal translocations in humans. DNA Repair 5:1136–1145
25. Kurata M, Maesako Y, Ueda C, Nishikori M, Akasaka T, Uchiyama T, Ohno H (2002) Characterization of t(3;6)(q27;p21) breakpoints in B-cell non-Hodgkin's lymphoma and construction of the histone H4/BCL6 fusion gene, leading to altered expression of Bcl-6. Can Res 62:6224–6230
26. Leach DRF, Stahl FW (1983) Viability of λ phages carrying a perfect palindrome in the absence of recombination nucleases. Nature 305:448–451
27. Limanskaia O, Limanskiĭ AP (2009) Distribution of potentially hairpin-loop structures in the genome of bovine retroviruses. Vopr Virusol 54:27–32
28. Lu Z, Tsai AG, Akasaka T, Ohno H, Jiang Y, Melnick AM, Greisman HA, Lieber MR (2013) BCL6 breaks occur at different AID sequence motifs in Ig-BCL6 and non-Ig-BCL6 rearrangements. Blood 121:4551–4554
29. Marculescu R, Le T, Simon P, Jaeger U, Nadel B (2002) V(D)J-mediated translocations in lymphoid neoplasms: a functional assessment of genomic instability by cryptic sites. J Exp Med 195:85–98
30. Mirkin SM (2007) Expandable DNA repeats and human disease. Nature 447:932–940
31. Musso M, Bianchi-Scarrà G, Van Dyke MW (2000) The yeast CDP1 gene encodes a triple-helical DNA-binding protein. Nucleic Acids Res 28:4090–4096
32. Naik AK, Raghavan SC (2008) P1 nuclease cleavage is dependent on length of the mismatches in DNA. DNA Repair 7:1384–1391
33. Nakamura Y, Takahashi N, Kakegawa E, Yoshida K, Ito Y, Kayano H, Niitsu N, Jinnai I, Bessho M (2008) The GAS5 (growth arrest-specific transcript 5) gene fuses to BCL6 as a result of t(1;3)(q25;q27) in a patient with B-cell lymphoma. Cancer Genet Cytogenet 182:144–149
34. Nambiar M, Goldsmith G, Moorthy BT, Lieber MR, Joshi MV, Choudhary B, Hosur RV, Raghavan SC (2011) Formation of a G-quadruplex at the BCL2 major breakpoint region of the t(14;18) translocation in follicular lymphoma. Nucleic Acids Res 39:936–948
35. Nambiar M, Raghavan SC (2011) How does DNA break during chromosomal translocations? Nucleic Acids Res 39:5813–5825
36. Nambiar M, Raghavan SC (2012) Mechanism of fragility at BCL2 gene minor breakpoint cluster region during t(14;18) chromosomal translocation. J Biol Chem 287:8688–8701
37. Nambiar M, Raghavan SC (2013) Chromosomal translocations among the healthy human population: implications in oncogenesis. Cell Mol Life Sci 70:1381–1392
38. Nambiar M, Srivastava M, Gopalakrishnan V, Sankaran SK, Raghavan SC (2013) G-quadruplex structures formed at the HOX11 breakpoint region contribute to its fragility during t(10;14) translocation in T-cell leukemia. Mol Cell Biol 33:4266–4281
39. Niu H, Cattoretti G, Dalla-Favera R (2003) BCL6 controls the expression of the B7–1/CD80 costimulatory receptor in germinal center B cells. J Exp Med 198:211–221
40. Noer SL, Preus S, Gudnason D, Aznauryan M, Mergny JL, Birkedal V (2016) Folding dynamics and conformational heterogeneity of human telomeric G-quadruplex structures in Na+ solutions by single molecule FRET microscopy. Nucleic Acids Res 44:464–471
41. Onizuka T, Moriyama M, Yamochi T, Kuroda T, Kazama A, Kanazawa N, Sato K, Kato T, Ota H, Mori S (1995) BCL-6 gene product, a 92- to 98-kD nuclear phosphoprotein, is highly expressed in germinal center B cells and their neoplastic counterparts. Blood 86:28–37
42. Pasqualucci L, Migliazza A, Basso K, Houldsworth J, Chaganti RS, Dalla-Favera R (2003) Mutations of the BCL6 proto-oncogene disrupt its negative autoregulation in diffuse large B-cell lymphoma. Blood 101:2914–2923
43. Phan RT, Dalla-Favera R (2004) The BCL6 proto-oncogene suppresses p53 expression in germinal-centre B cells. Nature 432:635–639
44. Raghavan SC, Houston S, Hegde BG, Langen R, Haworth IS, Lieber MR (2004) Stability and strand asymmetry in the non-B DNA structure at the bcl-2 major breakpoint region. J Biol Chem 279:46213–46225
45. Raghavan SC, Kirsch IR, Lieber MR (2001) Analysis of the V(D)J recombination efficiency at lymphoid chromosomal translocation breakpoints. J Biol Chem 276:29126–29133
46. Raghavan SC, Lieber MR (2004) Chromosomal translocations and non-B DNA structures in the human genome. Cell Cycle (Georgetown, Tex.) 3:762–768
47. Saito M, Gao J, Basso K, Kitagawa Y, Smith PM, Bhagat G, Pernis A, Pasqualucci L, Dalla-Favera R (2007) A signaling pathway mediating downregulation of BCL6 in germinal center B cells is blocked by BCL6 gene alterations in B cell lymphoma. Cancer Cell 12:280–292
48. Sharma S, Doherty KM, Brosh RM Jr (2006) Mechanisms of RecQ helicases in pathways of DNA metabolism and maintenance of genomic stability. Biochem J 398:319–337
49. Sommers JA, Rawtani N, Gupta R, Bugreev DV, Mazin AV, Cantor SB, Brosh RM Jr (2009) FANCJ uses its motor ATPase to destabilize protein-DNA complexes, unwind triplexes, and inhibit RAD51 strand exchange. J Biol Chem 284:7505–7517
50. Susanibar-Adaniya S, Barta SK (2021) 2021 update on diffuse large B cell lymphoma: a review of current data and potential applications on risk stratification and management. Am J Hematol 96:617–629
51. Testoni M, Zucca E, Young KH, Bertoni F (2015) Genetic lesions in diffuse large B-cell lymphomas. Ann Oncol 26:1069–1080
52. Ueda C, Akasaka T, Kurata M, Maesako Y, Nishikori M, Ichinohasama R, Imada K, Uchiyama T, Ohno H (2002) The gene for

interleukin-21 receptor is the partner of BCL6 in t(3;16)(q27;p11), which is recurrently observed in diffuse large B-cell lymphoma. Oncogene 21:368–376
53. Ueda C, Akasaka T, Ohno H (2002) Non-immunoglobulin/BCL6 gene fusion in diffuse large B-cell lymphoma: prognostic implications. Leuk Lymphoma 43:1375–1381
54. Vega F, Medeiros LJ (2003) Chromosomal translocations involved in non-Hodgkin lymphomas. Arch Pathol Lab Med 127:1148–1160
55. Wang X, Li Z, Naganuma A, Ye BH (2002) Negative autoregulation of BCL-6 is bypassed by genetic alterations in diffuse large B cell lymphomas. Proc Natl Acad Sci 99:15018–15023
56. Wu Y, Shin-ya K, Brosh RM Jr (2008) FANCJ helicase defective in Fanconia anemia and breast cancer unwinds G-quadruplex DNA to defend genomic stability. Mol Cell Biol 28:4116–4128
57. Xu WS, Liang RHS, Srivastava G (2000) Identification and characterization of BCL6 translocation partner genes in primary gastric high-grade B-cell lymphoma: Heat shock protein 89 alpha is a novel fusion partner gene of BCL6. Genes Chromosom Cancer 27:69–75
58. Ye BH, Cattoretti G, Shen Q, Zhang J, Hawe N, de Waard R, Leung C, Nouri-Shirazi M, Orazi A, Chaganti RS et al (1997) The BCL-6 proto-oncogene controls germinal-centre formation and Th2-type inflammation. Nat Genet 16:161–170
59. Ye BH, Rao PH, Chaganti RS, Dalla-Favera R (1993) Cloning of bcl-6, the locus involved in chromosome translocations affecting band 3q27 in B-cell lymphoma. Cancer Res 53:2732–2735
60. Yonetani N, Akasaka T, Akasaka H, Ohno H, Okuma M, Miura I, Takahashi N, Miyanishi S, Okumura A, Muramatsu M et al (1998) Molecular features of a new human lymphoma cell line carrying both BCL2 and BCL6 gene rearrangements. Oncogene 17:971–979
61. Yoshida T, Fukuda T, Hatano M, Koseki H, Okabe S, Ishibashi K, Kojima S, Arima M, Komuro I, Ishii G et al (1999) The role of Bcl6 in mature cardiac myocytes. Cardiovasc Res 42:670–679
62. Zeleznik-Le NJ, Harden AM, Rowley JD (1994) 11q23 translocations split the "AT-hook" cruciform DNA-binding region and the transcriptional repression domain from the activation domain of the mixed-lineage leukemia (MLL) gene. Proc Natl Acad Sci USA 91:10610–10614
63. Zuker M (2003) Mfold web server for nucleic acid folding and hybridization prediction. Nucleic Acids Res 31:3406–3415